Inorg. Chem. **2006**, *45*, 4484–4496

Lanthanide(III) Complexes with a Tetrapyridine Pendant-Armed Macrocyclic Ligand: ^{1}H NMR Structural Determination in Solution, X-ray Diffraction, and Density-Functional Theory Calculations

M. del C. Fernández-Fernández,[†] R. Bastida,*[,†] A. Macías,[†] P. Pérez-Lourido,[‡] C. Platas-Iglesias,*[,§] and L. Valencia*[,†]

Departamento de Química Inorgánica, Facultad de Química, Universidad de Santiago de Compostela, Avda. de las Ciencias s/n, E-15782, Santiago de Compostela, Spain, Departamento de Química Inorgánica, Facultad de Ciencias, Universidade de Vigo, Marcosende, Pontevedra, Spain, and Departamento de Química Fundamental, Facultade de Ciencias, Universidade da Coruña, A Coruña, Spain

Received March 2, 2006

Complexes between the tetrapyridyl pendant-armed macrocyclic ligand (**L**) and the trivalent lanthanide ions have been synthesized, and structural studies have been made both in the solid state and in aqueous solution. The crystal structures of the La, Ce, Pr, Gd, Tb, Er, and Tm complexes have been determined by single-crystal X-ray crystallography. In the solid state, all the cation complexes show a 10-coordinated geometry close to a distorted bicapped antiprism, with the pyridine pendants situated alternatively above and below the main plane of the macrocycle. The conformations of the two five-membered chelate rings present in the complexes change along the lanthanide series. The La(III) and Ce(III) complexes show a $\lambda\delta$ (or $\delta\lambda$) conformation, while the complexes of the heavier lanthanide ions present $\lambda\lambda$ (or $\delta\delta$) conformation. The cationic $[Ln(\mathbf{L})]^{3+}$ complexes (Ln = La, Pr, Eu, Tb, and Tm) were also characterized by theoretical calculations at the density-functional theory (DFT) B3LYP level. The theoretical calculations predict a stabilization of the $\lambda\lambda$ (or $\delta\delta$) conformation on decreasing the ionic radius of the Ln(III) ion, in agreement with the experimental evidence. The solution structures show a good agreement with the calculated ones, as demonstrated by paramagnetic NMR measurements (lanthanide induced shifts and relaxation rate enhancements). The ^{1}H NMR spectra indicate an effective D_2 symmetry of the complexes in D_2O solution. The ^{1}H lanthanide induced shifts (LIS) observed for the Ce(III), Tm(III), and Yb(III) complexes can be fit to a theoretical model assuming that dipolar contributions are dominant for all protons. The resulting calculated values are consistent with highly rhombic magnetic susceptibility tensors with the magnetic axes being coincident with the symmetry axes of the molecule. In contrast with the solid-state structure, the analysis of the LIS data indicates that the Ce(III) complexes present a $\lambda\lambda$ (or $\delta\delta$) conformation in solution.

Introduction

Over the past decade, a large effort has been devoted to the rational design and synthesis of organic polydentate ligands capable of forming stable lanthanide complexes in aqueous solutions, because of the successful applications of Ln(III) systems in medicine and biology. The use of contrast agents in magnetic resonance imaging (MRI) has become an important tool in modern medical diagnostics.[1] Contrast agents significantly improve the image by enhancing the nuclear magnetic relaxation rates of water protons in the tissues where they are distributed.[2,3] Because of the high magnetic moment (seven unpaired electrons) and the relatively long electronic relaxation time of the metal ion,

* To whom correspondence should be addressed. E-mail: qilaura@usc.es (C.P.-I.), qibastid@usc.es (R.B. and L.V.).
[†] Universidad de Santiago de Compostela.
[‡] Universidade de Vigo.
[§] Universidade da Coruña.

(1) *The Chemistry of Contrast Agents in Medical Magnetic Resonance Imaging;* Mebach, A. E., Tóth, É., Eds.; Wiley: New York, 2001.
(2) Comblin, V.; Gilsoul, D.; Hermann, M.; Humblet, V.; Jacques, V.; Mesbahi, M.; Sauvage, C.; Desreux, J. F. *Coord. Chem. Rev.* **1999**, *185−186*, 451.
(3) Caravan, P.; Ellison, J. J.; McMurry, T. J.; Lauffer, R. B.; *Chem. Rev.* **1999**, *99*, 2293.

10.1021/ic0603508 CCC: $33.50
Published on Web 05/02/2006

complexes of Gd(III) are currently the most employed in clinical practice as contrast agents.[4] Lanthanide(III) complexes also have important applications in diagnostic[5] and therapeutic radiopharmaceuticals[6] and as luminescent probes to investigate biomedical systems.[7]

Because the free Ln(III) ions are very toxic, a prerequisite for their in vivo application is its complexation with polydentate ligands to form compounds of high kinetic and thermodynamic stability in order to prevent dissociation. If the kinetic inertness in aqueous solution is a shared prerequisite for lanthanide complexes used as MRI contrast agents or luminescent bioprobes, it should be noted that the denticity requirement for the chelator is not the same in these two systems. The Gd(III) complex should have at least one vacant inner-sphere coordination site for water−ligand exchange to enhance the water proton-relaxation rates. In contrast, Eu(III) or Tb(III) ions should be fully shielded from surrounding water molecules, which contribute to nonradiative deexcitation and a reduced quantum yield for lanthanide luminescence.

Polyazamacrocycles with coordinating pendant arms form very stable complexes with a wide range of metal ions, including Ln(III) ions. These ligands encapsulate the metal ion in the macrocyclic cavity providing to the complexes high thermodynamic and kinetic stabilities. The most widely studied ligands of this type used to prepare Gd(III)-based MRI contrast agents or photoactive Eu(III) and Tb(III) chelates are based on the 12-membered tetraazamacrocycle cyclen, which can be functionalized with acetate or propionate side chains.[2−8] However, less effort has been made on the preparation of Ln(III) chelates with macrocyclic ligands containing pyridine units.[9] Introduction of pyridine moieties into an azamacrocyclic skeleton is expected to increase the conformational rigidity of the macrocycle and therefore to change the selectivity and coordinative properties of the ligand.

In previous work we have reported a solution ^{1}H NMR and solid-state study of Ln(III) complexes with a macrocyclic $Py_2N_6Ac_4$ ligand containing four carboxylate pendant groups **L**$^{\mathbf{1}}$ (Chart 1).[10] The solid-state structures of the complexes showed a 10-coordinate geometry for the lighter lanthanide ions La(III)−Dy(III), while for the heavier ions the X-ray structures showed a 9-coordinate geometry with one of the carboxylate pendant groups uncoordinated. The solution structures obtained were in agreement with a 10-coordinate geometry for La(III)−Dy(III) and 9-coordinate for Tm(III) and Lu(III) but showed that the 10-coordinate structure was still exclusive in solution for the Ho(III) complex and predominant for the Er(III) one. Herein, we report the Ln(III) and Y(III) complexes of the tetrapyridyl pendant-armed macrocyclic ligand **L** (Chart 1). The corresponding lanthanide complexes were characterized by solid-state X-ray diffraction studies and by theoretical calculations at the DFT (density-functional theory) level.

Chart 1

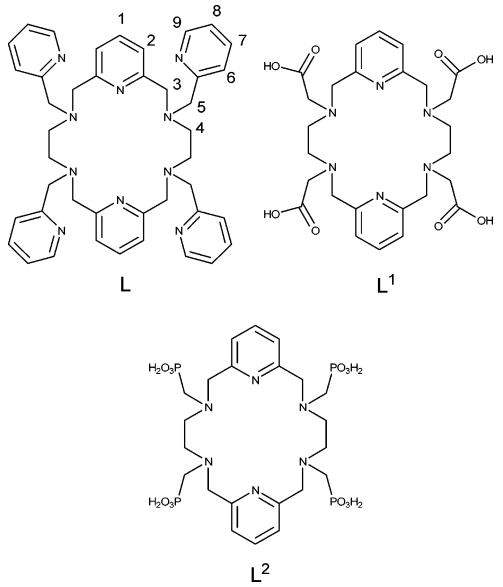

Most Ln(III) ions are paramagnetic and thus induce substantial chemical shifts in the ^{1}H NMR signals of protons located in the vicinity of the metal center.[11] On a fundamental level, the lanthanide induced shifts (LIS) arise from the interaction of the relevant nuclear and electronic spins that can be separated into through-space (dipolar) and through-bonds (contact) contributions. The dipolar contribution is dependent on the magnetic anisotropy of the complex in question and the position in space of a given proton and thus can be used to obtain structural information in solution. Furthermore, the binding of a ligand to a paramagnetic Ln(III) ion induces relaxation rate enhancement effects (LIR) that are related to the distance between the observed nucleus and the Ln(III) ion.[11] Thus, the solution structures of [Ln(**L**)]$^{3+}$ complexes were studied by ^{1}H NMR techniques in D_2O solution. The structural information obtained in solution from the LIS and LIR data was compared to the solid state structures and to the theoretically optimized geometries of the [Ln(**L**)]$^{3+}$ complexes.

Experimental Section

Measurements. Elemental analyses were performed in a Carlo-Erba EA microanalyzer. Infrared (IR) spectra were recorded as a KBr disks on a Bruker IFS-66V. LSI-MS spectra were recorded using a Micromass Autospec spectrometer with 3-nitrobenzyl alcohol as the matrix. ^{1}H NMR spectra were recorded in D_2O solutions, on Bruker DPX 250, Varian Unity 300 and 400, and Bruker AMX 500 NMR spectrometers, operating at 250.13, 300.13, 399.90, and 499.80 MHz, respectively. Longitudinal ^{1}H relaxation

(4) Aime, S.; Botta, M.; Fasano, M.; Terreno, E. *Chem. Soc. Rev.* **1998**, *27*, 19.
(5) Anderson, C. J.; Welch, M. J.; *Chem. Rev.* **1999**, *99*, 2219.
(6) Guo, Z.; Sadler, P. J. *Angew. Chem., Int. Ed.* **1999**, *38*, 1512.
(7) Bornhop, D. J.; Hubbard, D. S.; Houlne, M. P.; Adair, C.; Kiefer, G. E.; Pence, B. C.; Morgan, D. L. *Anal. Chem.* **1999**, *71*, 2607.
(8) Lecomte, C.; Dahaoui-Gindrey, V.; Chollet, H.; Gros, C.; Mishra, A. K.; Barbette, F.; Pullumbi, P.; Guilard, R. *Inorg. Chem.* **1997**, *36*, 3827.
(9) Aime, S.; Gianolio, E.; Corpillo, D.; Cavallotti, C.; Palmisano, M.; Sisti, M.; Giovenzana, G. B.; Pagliarin, R. *Helv. Chim. Acta* **2003**, *86*, 615.
(10) Valencia, L.; Martínez, J.; Macías, A.; Bastida, R.; Carvalho R. A.; Geraldes C. F. G. C. *Inorg. Chem.* **2002**, *41*, 5300.
(11) Peters, J. A.; Huskens J.; Raber, D. J. *Prog. Nucl. Magn. Res. Spectrosc.* **1996**, *28*, 283.

times (T_1) were measured by the inversion−recovery pulse sequence.[12] Transverse relaxation times (T_2) were measured from the width of the peaks at half-height. The paramagnetic contributions to the relaxation rates were corrected for diamagnetic effects using the T_1 values and the line widths for the La(III) complex under the same experimental conditions. ^{1}H NMR spectra of the La(III)−Eu(III) complexes were assigned with the aid of two-dimensional COSY experiments.

Materials. Pyridine-2,6-dicarbaldehyde was prepared according to literature procedures.[13] Pycolyl chloride hydrochloride, ethylendiamine, and hydrated lanthanide(III) and yttrium(III) nitrates were obtained from Aldrich. Solvents used were of reagent grade and purified by the usual methods. D_2O (99.8% D) was obtained from Sigma. The ligand **L** was synthesized as previously reported by our research group.[14]

Preparation of the Complexes. A solution of $Ln(NO_3)_3 \cdot xH_2O$ or $Y(NO_3)_3 \cdot 4H_2O$ (1 mmol) in acetonitrile (10 mL) was added dropwise to a stirred solution of **L** (0.345 g, 0.5 mmol) in acetonitrile (25 mL). After the addition was completed, the resulting colorless solution was stirred for 2 h and concentrated in the rotary evaporator until ca. 10 mL. The solution was allowed to precipitate, and the precipitate formed was filtered off yielding the lanthanide complexes of the ligand.

La[La(L)](NO$_3$)$_6$·2H$_2$O (1). Anal. Calcd for $C_{42}H_{50}N_{16}O_{20}La_2$: C, 36.6; H, 3.7; N, 16.3. Found: C, 36.6; H, 3.8; N, 16.1%. Yield: 60%. IR (KBr, cm^{-1}): 1570, 1604 [ν(C=C) and $\nu(C{=}N)_{py}$], 1335, 1384, 1455 [$\nu(NO_3^-)$]. Crystals of formula [La(**L**)][La(NO$_3$)$_6$]·0.5CH$_3$CN·0.5H$_2$O suitable for X-ray diffraction were grown from an acetonitrile solution of the isolated solid.

Ce[Ce(L)](NO$_3$)$_6$·2H$_2$O (2). Anal. Calcd for $C_{42}H_{50}N_{16}O_{20}Ce_2$: C, 36.6; H, 3.7; N, 16.3. Found: C, 36.3; H, 3.9; N, 16.5%. Yield: 82%. IR (KBr, cm^{-1}): 1571, 1605 [ν(C=C) and $\nu(C{=}N)_{py}$], 1330, 1384, 1455 [$\nu(NO_3^-)$]. MS (LSI-MS, *m*/*z*): 954 [Ce**L**(NO$_3$)$_2$]$^+$, 893 [Ce**L**(NO$_3$)]$^+$. Crystals of formula [Ce(**L**)][Ce(NO$_3$)$_6$]·0.5CH$_3$CN·0.5H$_2$O suitable for X-ray diffraction were grown from an acetonitrile solution of the isolated solid.

Pr[Pr(L)](NO$_3$)$_6$·3H$_2$O (3). Anal. Calcd for $C_{42}H_{52}N_{16}O_{21}Pr_2$: C, 36.1; H, 3.8; N, 16.0. Found: C, 36.0; H, 3.8; N, 16.4%. Yield: 85%. IR (KBr, cm^{-1}): 1570, 1605 [ν(C=C) and $\nu(C{=}N)_{py}$], 1326, 1384, 1456 [$\nu(NO_3^-)$]. MS (LSI-MS, *m*/*z*): 1282 [Pr$_2$**L**(NO$_3$)$_5$]$^+$, 955 [Pr**L**(NO$_3$)$_2$]$^+$, 894 [Pr**L**(NO$_3$)]$^+$. Crystals of formula [Pr(**L**)][Pr(NO$_3$)$_6$]·2CH$_3$CN·1.5H$_2$O suitable for X-ray diffraction were grown from an acetonitrile solution of the isolated solid.

Nd[Nd(L)](NO$_3$)$_6$·2H$_2$O (4). Anal. Calcd for $C_{42}H_{50}N_{16}O_{20}Nd_2$: C, 36.4; H, 3.6; N, 16.2. Found: C, 36.7; H, 3.9; N, 16.1%. Yield: 87%. IR (KBr, cm^{-1}): 1571, 1605 [ν(C=C) and $\nu(C{=}N)_{py}$], 1306, 1384, 1457 [$\nu(NO_3^-)$]. MS (LSI-MS, *m*/*z*): 1288 [Nd$_2$**L**(NO$_3$)$_5$]$^+$, 958 [Nd**L**(NO$_3$)$_2$]$^+$, 896 [Nd**L**(NO$_3$)]$^+$.

Sm[Sm(L)](NO$_3$)$_6$·2H$_2$O (5). Anal. Calcd for $C_{42}H_{50}N_{16}O_{20}Sm_2$: C, 36.0; H, 3.6; N, 16.0. Found: C, 36.6; H, 3.8; N, 15.8%. Yield: 80%. IR (KBr, cm^{-1}): 1571, 1605 [ν(C=C) and $\nu(C{=}N)_{py}$], 1304, 1384, 1458 [$\nu(NO_3^-)$]. MS (LSI-MS, *m*/*z*): 966 [Sm**L**(NO$_3$)$_2$]$^+$, 905 [Sm**L**(NO$_3$)]$^+$.

Eu[Eu(L)](NO$_3$)$_6$·2H$_2$O (6). Anal. Calcd for $C_{42}H_{50}N_{16}O_{20}Eu_2$: C, 36.0; H, 3.6; N, 16.0. Found: C, 36.2; H, 4.0; N, 16.7%. Yield: 82%. IR (KBr, cm^{-1}): 1571, 1606 [ν(C=C) and $\nu(C{=}N)_{py}$], 1305, 1384, 1459 [$\nu(NO_3^-)$]. MS (LSI-MS, *m*/*z*): 1242 [Eu$_2$**L**(NO$_3$)$_4$]$^+$, 967 [Eu**L**(NO$_3$)$_2$]$^+$, 905 [Eu**L**(NO$_3$)]$^+$.

Gd[Gd(L)](NO$_3$)$_6$·4H$_2$O (7). Anal. Calcd for $C_{42}H_{54}N_{16}O_{22}Gd_2$: C, 34.8; H, 3.8; N, 15.5. Found: C, 35.0; H, 3.9; N, 15.1%. Yield: 80%. IR (KBr, cm^{-1}): 1571, 1608 [ν(C=C) and $\nu(C{=}N)_{py}$], 1305, 1384, 1459 [$\nu(NO_3^-)$]. MS (LSI-MS, *m*/*z*): 972 [Gd**L**(NO$_3$)$_2$]$^+$. Crystals of formula [Gd(**L**)][Gd(NO$_3$)$_4$(H$_2$O)$_2$]·2NO$_3$·2H$_2$O suitable for X-ray diffraction were grown from an acetonitrile solution of the isolated solid.

Tb[Tb(L)](NO$_3$)$_6$·2H$_2$O (8). Anal. Calcd for $C_{42}H_{50}N_{16}O_{20}Tb_2$: C, 35.6; H, 3.6; N, 15.8. Found: C, 35.6; H, 3.8; N, 16.1%. Yield: 80%. IR (KBr, cm^{-1}): 1573, 1607 [ν(C=C) and $\nu(C{=}N)_{py}$], 1306, 1384, 1460 [$\nu(NO_3^-)$]. MS (LSI-MS, *m*/*z*): 973 [Tb**L**(NO$_3$)$_2$]$^+$. Crystals of formula [Tb(**L**)][Tb(NO$_3$)$_6$]·2CH$_3$CN suitable for X-ray diffraction were grown from an acetonitrile solution of the isolated solid.

Dy[Dy(L)](NO$_3$)$_6$·3H$_2$O (9). Anal. Calcd for $C_{42}H_{52}N_{16}O_{21}Dy_2$: C, 35.0; H, 3.6; N, 15.5. Found: C, 35.3; H, 3.9; N, 15.0%. Yield: 72%. IR (KBr, cm^{-1}): 1574, 1610 [ν(C=C) and $\nu(C{=}N)_{py}$], 1304, 1384, 1465 [$\nu(NO_3^-)$]. MS (LSI-MS, *m*/*z*): 978 [Dy**L**(NO$_3$)$_2$]$^+$.

Ho[Ho(L)](NO$_3$)$_6$·H$_2$O (10). Anal. Calcd for $C_{42}H_{52}N_{16}O_{21}Ho_2$: C, 34.9; H, 3.6; N, 15.5. Found: C, 34.3; H, 3.7; N, 15.0%. Yield: 80%. IR (KBr, cm^{-1}): 1574, 1610 [ν(C=C) and $\nu(C{=}N)_{py}$], 1305, 1384, 1474 [$\nu(NO_3^-)$]. MS (LSI-MS, *m*/*z*): 1330 [Ho$_2$**L**(NO$_3$)$_5$]$^+$, 979 [Ho**L**(NO$_3$)$_2$]$^+$.

Er[Er(L)](NO$_3$)$_6$·2H$_2$O (11). Anal. Calcd for $C_{42}H_{50}N_{16}O_{20}Er_2$: C, 35.2; H, 3.5; N, 15.6. Found: C, 35.3; H, 3.3; N, 16.1%. Yield: 63%. IR (KBr, cm^{-1}): 1571, 1610 [ν(C=C) and $\nu(C{=}N)_{py}$], 1307, 1384, 1440 [$\nu(NO_3^-)$]. MS (LSI-MS, *m*/*z*): 1334 [Er$_2$**L**(NO$_3$)$_5$]$^+$, 982 [Er**L**(NO$_3$)$_2$]$^+$. Crystals of formula [Er(**L**)][Er(NO$_3$)$_3$(H$_2$O)$_3$]·3NO$_3$·3H$_2$O suitable for X-ray diffraction were grown from an acetonitrile solution of the isolated solid.

Tm[Tm(L)](NO$_3$)$_6$·4H$_2$O (12). Anal. Calcd for $C_{42}H_{54}N_{16}O_{22}Tm_2$: C, 34.3; H, 3.7; N, 15.2. Found: C, 34.1; H, 3.2; N, 16.0%. Yield: 80%. IR (KBr, cm^{-1}): 1574, 1611 [ν(C=C) and $\nu(C{=}N)_{py}$], 1305, 1384, 1467 [$\nu(NO_3^-)$]. MS (LSI-MS, *m*/*z*): 983 [Tm**L**(NO$_3$)$_2$]$^+$. Crystals of formula [Tm(**L**)][Tm(NO$_3$)$_3$(H$_2$O)$_3$]3NO$_3$·3H$_2$O suitable for X-ray diffraction were grown from an acetonitrile solution of the isolated solid.

Yb[Yb(L)](NO$_3$)$_6$·3H$_2$O (13). Anal. Calcd for $C_{42}H_{52}N_{16}O_{21}Yb_2$: C, 34.5; H, 3.6; N, 15.3. Found: C, 34.6; H, 3.2; N, 15.1%. Yield: 75%. IR (KBr, cm^{-1}): 1574, 1610 [ν(C=C) and $\nu(C{=}N)_{py}$], 1307, 1384, 1440 [$\nu(NO_3^-)$]. MS (LSI-MS, *m*/*z*): 1346 [Yb$_2$**L**(NO$_3$)$_5$]$^+$, 988 [Yb**L**(NO$_3$)$_2$]$^+$, 926 [Yb**L**(NO$_3$)]$^+$.

Y[Y(L)](NO$_3$)$_6$·3H$_2$O (14). Anal. Calcd for $C_{42}H_{52}N_{16}O_{21}Y_2$: C, 39.0; H, 4.1; N, 17.3. Found: C, 38.6; H, 4.2; N, 17.5%. Yield: 54%. IR (KBr, cm^{-1}): 1575, 1609 [ν(C=C) and $\nu(C{=}N)_{py}$], 1305, 1384, 1445 [$\nu(NO_3^-)$]. MS (LSI-MS, *m*/*z*): 843 [Y**L**(NO$_3$)]$^+$.

Crystal Structure Determination of Complexes. Colorless prisms of the complexes were obtained by slow recrystallization of the compounds in acetonitrile and used for the structure determination. The details of the X-ray crystal structure solution and refinement are given in Table 1. Measurements were made on a Bruker SMART CCD area detector. All data were corrected for Lorentz and polarization effects. An empirical absorption correction was also applied for all the crystal structures obtained.[15] Complex scattering factors were taken from the program package SHELXTL.[16] The structures were solved by direct methods, which revealed

(12) Vold, R. L.; Waugh, J. S.; Klein, M. P.; Phelps, D. E. *J. Chem. Phys.* **1968**, *48*, 3831.
(13) Alcock, N. W.; Kingston, R. G.; Moore, P.; Pierpoint, C. *J. Chem. Soc., Dalton Trans.* **1984**, 1937.
(14) Bastida, R.; Fenton, D. E.; López-Deber, M.; Macías, A.; Valencia L.; Vicente, M. *Inorg. Chim. Acta* **2003**, *355*, 292.
(15) Sheldrick, G. M. *SADABS: Program for Empirical Absorption Correction for Area Detector Data;* University of Göttingen: Göttingen, Germany, 1996.

Table 1. Crystal Data and Structure Refinement for Compounds **1**−**3**, **7**, **8**, **11**, and **12**

	1	**2**	**3**	**7**	**8**	**11**	**12**
formula	$C_{43}H_{47.5}N_{16.5}O_{18.5}La_2$	$C_{43}H_{47.5}N_{16.5}O_{18.5}Ce_2$	$C_{46}H_{52}N_{18}O_{19.5}Pr_2$	$C_{42}H_{46}N_{16}O_{22}Gd_2$	$C_{46}H_{52}N_{18}O_{18}Tb_2$	$C_{42}H_{46}N_{16}O_{24}Er_2$	$C_{42}H_{46}N_{16}O_{24}Tm_2$
mol wt	1369.29	1371.71	1450.88	1441.45	1462.90	1493.47	1496.81
cryst syst	monoclinic	monoclinic	monoclinic	monoclinic	monoclinic	orthorrombic	orthorrombic
space group	*P*21/*n*	*P*21/*n*	*P*21/*c*	*P*21/*n*	*P*21/*c*	*Pbca*	*Pbca*
a (Å)	12.447(3)	12.406(2)	25.767(5)	14.2551(8)	25.760(5)	23.387(4)	23.496(10)
b (Å)	24.227(7)	24.226(4)	10.516(2)	20.9320(12)	11.354(2)	19.441(3)	19.495(8)
c (Å)	17.726(5)	17.742(3)	21.566(4)	17.6226(10)	19.085(4)	24.101(4)	24.189(10)
β (deg)	95.620(4)	95.738(3)	108.331(4)	92.8780(10)	104.791(3)		
V (Å^3)	5319(3)	5305.4(15)	5547.1(19)	5251.7(5)	5397.1(17)	10958(3)	11080(8)
Z	4	4	4	4	4	8	8
D_{calcd} (mg/m^3)	1.710	1.717	1.737	1.823	1.800	1.811	1.795
μ (mm^{-1})	1.673	1.783	1.828	2.600	2.690	3.140	3.278
R_{int}	0.1064	0.0326	0.0869	0.0712	0.0368	0.1490	0.1689
R1[a]	0.0768	0.0297	0.0502	0.0427	0.0280	0.0461	0.0991
wR2 (all data)[b]	0.2047	0.1061	0.1366	0.0973	0.0741	0.0914	0.2571

[a] $R1 = \sum||F_o| - |F_c||/\sum|F_o|$. [b] $wR2 = \{\sum[w(|F_o|^2 - |F_c|^2|)^2]/\sum[w(F_o^4|)]\}^{1/2}$.

the position of all non-hydrogen atoms. All the structures were refined on F^2 by a full-matrix least-squares procedure using anisotropic displacement parameters for all non-hydrogen atoms.[17] The hydrogen atoms were located in their calculated positions and refined using a riding model.

Analysis of the LIS Data. Lanthanide induced paramagnetic shifts (LIS) of $[Ln(\mathbf{L})]^{3+}$ complexes were calculated using the corresponding La(III) complex as a diamagnetic reference. The LIS values were analyzed by using the SHIFT ANALYSIS program developed by Forsberg,[18] where no assumption is made about the magnetic symmetry of the complex. The X-ray crystal structures of the Ce(III) and Pr(III) complexes, as defined by their Cartesian coordinates with the Ln(III) ion at the origin, were used as input structures for the analysis of the LIS values of Ce(III), Pr(III), and Nd(III) complexes. For the Tm(III) and Yb(III) complexes the X-ray structure of the Tm(III) complex was used as a structural model. B3LYP optimized structures of the Pr(III), Tb(III), and Tm(III) complexes in both $\delta\lambda$ and $\lambda\lambda$ conformations were also used as input geometries. The agreement factors between the observed and calculated values were determined according to eq 1:[19]

$$AF_i = [\sum_j (\delta_{ij}^{exp} - \delta_{ij}^{cal})^2 / \sum_j (\delta_{ij}^{exp})^2]^{1/2} \quad (1)$$

where δ_{ij}^{exp} and δ_{ij}^{cal} represent the experimental and calculated values of a nucleus *i* in a given Ln(III) complex *j*, respectively.

Computational Methods. All calculations were performed employing hybrid DFT with the B3LYP exchange-correlation functional[20,21] and the Gaussian 03 package (revision C.01).[22] Full geometry optimizations of the $[Ln(\mathbf{L})]^{3+}$ systems (Ln = La, Pr, Eu, Tb, or Tm) were performed in vacuo by using the effective core potential (ECP) of Dolg et al. and the related [5s4p3d]-GTO valence basis set for the lanthanides[23] and the 3-21G* basis set for C, H, and N atoms. Two geometries of the complexes showing different conformations of the two five-membered chelate rings formed by the ethylenediamine moieties were considered: $\delta\lambda$ and $\lambda\lambda$. The X-ray structures of the Ce ($\delta\lambda$) and Tm ($\lambda\lambda$) complexes were used as input geometries. The stationary points found on the potential energy surfaces as a result of the geometry optimizations have been tested to represent energy minima rather than saddle points via frequency analysis.

In aqueous solution relative free energies of the $\delta\lambda$ and $\lambda\lambda$ isomers were calculated from solvated single-point energy calculations on the geometries optimized in vacuo. In these calculations the 6-311G** basis set was used for C, H, and N atoms. Solvent effects were evaluated by using the polarizable continuum model (PCM). In particular, we used the C-PCM variant[24] that employs conductor rather than dielectric boundary conditions. The solute cavity is built as an envelope of spheres centered on atoms or atomic groups with appropriate radii. For lanthanides, the previously parametrized radii were used.[25] Free energies include both electrostatic and nonelectrostatic contributions.

Results and Discussion

Synthesis and Characterization of the Complexes. Reaction of **L** with the appropriate hydrated lanthanide nitrate in acetonitrile led to compounds of formula $M[M(\mathbf{L})](NO_3)_6 \cdot xH_2O$ (M = La−Yb and Y) in good yield (54−87%). The ligand reacted quickly with Ln(III) ions (except Lu(III)) producing kinetically stable complexes, which were characterized by elemental analysis, IR, NMR, and LSI-MS spectra. Attempts to prepare the corresponding Lu(III) complex by using analogous conditions were unsuccessful, the reaction of **L** with the Lu(III) salt giving rise to a crystalline product characterized as the macrocyclic ligand.

(16) *SHELXTL: An Integrated System for Solving and Refining Crystal Structures from Diffraction Data,* revision 5.1; Bruker, AXS Ltd.
(17) Sheldrick, G. M. *SHELXL-97: Program for the Refinement of Crystal Structures;* University of Göttingen: Göttingen, Germany, 1997.
(18) Forsberg, J. H.; Delaney, R. M.; Zhao, Q.; Harakas, G.; Chandran, R. *Inorg. Chem.* **1995**, *34*, 3705.
(19) Davis, R. E.; Willcott, M. R. *J. Am. Chem. Soc.* **1972**, *94*, 1744.
(20) Becke, A. D. *J. Chem. Phys.* **1993**, *98*, 5648.
(21) Lee, C.; Yang, W.; Parr, R. G. *Phys. Rev. B* **1988**, *37*, 785.
(22) Frisch, M. J.; Trucks, G. W.; Schlegel, H. B.; Scuseria, G. E.; Robb, M. A.; Cheeseman, J. R.; Montgomery, J. A., Jr.; Vreven, T.; Kudin, K. N.; Burant, J. C.; Millam, J. M.; Iyengar, S. S.; Tomasi, J.; Barone, V.; Mennucci, B.; Cossi, M.; Scalmani, G.; Rega, N.; Petersson, G. A.; Nakatsuji, H.; Hada, M.; Ehara, M.; Toyota, K.; Fukuda, R.; Hasegawa, J.; Ishida, M.; Nakajima, T.; Honda, Y.; Kitao, O.; Nakai, H.; Klene, M.; Li, X.; Knox, J. E.; Hratchian, H. P.; Cross, J. B.; Bakken, V.; Adamo, C.; Jaramillo, J.; Gomperts, R.; Stratmann, R. E.; Yazyev, O.; Austin, A. J.; Cammi, R.; Pomelli, C.; Ochterski, J. W.; Ayala, P. Y.; Morokuma, K.; Voth, G. A.; Salvador, P.; Dannenberg, J. J.; Zakrzewski, V. G.; Dapprich, S.; Daniels, A. D.; Strain, M. C.; Farkas, O.; Malick, D. K.; Rabuck, A. D.; Raghavachari, K.; Foresman, J. B.; Ortiz, J. V.; Cui, Q.; Baboul, A. G.; Clifford, S.; Cioslowski, J.; Stefanov, B. B.; Liu, G.; Liashenko, A.; Piskorz, P.; Komaromi, I.; Martin, R. L.; Fox, D. J.; Keith, T.; Al-Laham, M. A.; Peng, C. Y.; Nanayakkara, A.; Challacombe, M.; Gill, P. M. W.; Johnson, B.; Chen, W.; Wong, M. W.; Gonzalez, C.; Pople, J. A. *Gaussian 03*, revision C.01; Gaussian, Inc.: Wallingford, CT, 2004.
(23) Dolg, M.; Stoll, H.; Savin, A.; Preuss, H. *Theor. Chim. Acta* **1989**, *75*, 173.
(24) Barone, V.; Cossi, M. *J. Phys. Chem. A* **1998**, *102*, 1995.
(25) Cosentino, U.; Villa, A.; Pitea, D.; Moro, G.; Barone, V. *J. Phys. Chem. B* **2000**, *104*, 8001.

Table 2. Selected Bond Lengths (Å) of the Metal Coordination Environment in $[Ln(\mathbf{L})]^{3+}$ Cations Obtained from the X-ray Crystal Structures of **1**−**3**, **7**, **8**, **11**, and **12**

	[La-(**L**)]$^{3+}$	[Ce-(**L**)]$^{3+}$	[Pr-(**L**)]$^{3+}$	[Gd-(**L**)]$^{3+}$	[Tb-(**L**)]$^{3+}$	[Er-(**L**)]$^{3+}$	[Tm-(**L**)]$^{3+}$
N(1)−Ln(1)	2.677(8)	2.669(3)	2.615(5)	2.532(4)	2.546(2)	2.535(6)	2.566(13)
N(2)−Ln(1)	2.800(8)	2.739(3)	2.679(5)	2.663(4)	2.667(2)	2.617(7)	2.640(11)
N(3)−Ln(1)	2.761(8)	2.739(3)	2.686(5)	2.642(4)	2.648(2)	2.659(6)	2.674(12)
N(4)−Ln(1)	2.710(8)	2.706(3)	2.611(6)	2.551(4)	2.550(2)	2.524(6)	2.537(12)
N(5)−Ln(1)	2.739(8)	2.760(3)	2.689(6)	2.664(4)	2.660(2)	2.652(6)	2.660(12)
N(6)−Ln(1)	2.763(7)	2.772(3)	2.693(5)	2.660(4)	2.657(2)	2.628(7)	2.641(12)
N(7)−Ln(1)	2.810(7)	2.839(3)	2.810(5)	2.791(4)	2.838(2)	2.731(7)	2.751(13)
N(8)−Ln(1)	2.758(9)	2.743(3)	2.788(6)	2.764(4)	2.748(2)	2.766(7)	2.784(13)
N(9)−Ln(1)	2.757(9)	2.748(3)	2.769(6)	2.787(4)	2.721(2)	2.825(7)	2.850(15)
N(10)−Ln(1)	2.835(8)	2.743(3)	2.845(5)	2.794(4)	2.773(2)	2.678(7)	2.689(13)

The IR spectra recorded as KBr disks show similar features for all compounds. The spectra feature split bands associated with ν(C═N) and ν(C═C) vibrations of the pyridine rings, which are shifted to higher wavenumbers by complexation because of the interaction between the metal ions and the pyridinic nitrogen atoms.[26] In all complexes, the band at 1383 cm^{-1} associated with the presence of ionic nitrate is accompanied by several bands that clearly identify the presence of coordinated nitrate groups.[27] The mass spectrum (LSI-MS) of most compounds displays peaks corresponding to the $[Ln_2\mathbf{L}(NO_3)_5]^+$, $[Ln\mathbf{L}(NO_3)_2]^+$, or $[Ln\mathbf{L}(NO_3)]^+$ fragments, which confirms the formation of the lanthanide complexes.

X-ray Crystal Structures. The solid-state structures of compounds **1**, **2**, **3**, **7**, **8**, **11**, and **12** were determined by single-crystal X-ray diffraction analyses. Compounds **1**, **2**, **3**, **7**, and **8** crystallize in the monoclinic space group $P2_1/n$, while compounds **11** and **12** are isomorphous within the orthorhombic *Pbca* group. In all cases, the asymmetric unit consists of two different lanthanide complexes: the cation complex $[Ln(\mathbf{L})]^{3+}$ and the anion complex $[Ln(NO_3)_m(H_2O)_n]^{x-}$ (Ln = La, Ce, Pr, Gd, Tb, Er, and Tm). Acetonitrile and/or hydration water molecules are present in the crystal lattice in all cases, and crystals of **7**, **11**, and **12** also contain well-separated nitrate anions. Selected bond lengths of the lanthanide coordination environment in the $[Ln(\mathbf{L})]^{3+}$ cations are given in Table 2, while bond angles of the lanthanide coordination sphere are given in Table 1S (Supporting Information). ORTEP plots of $[Ln(\mathbf{L})]^{3+}$ complexes are shown in Figures 1 (Ln = La) and 2 (Ln = Tm). Molecular structures of the $[Ln(\mathbf{L})]^{3+}$ cations in compounds **2**, **3**, **7**, **8**, and **11** are shown in Figures 1S−5S (Supporting Information).

The X-ray structures demonstrate that the complexation of the metal ion by the tetrapyridyl-armed macrocycle affords 10-coordinate mononuclear structures, with the metal ion being bound to all the nitrogen donor atoms of the ligand (six nitrogen donor atoms of the macrocyclic backbone and four nitrogen atoms of the pyridine pendant arms). The four pyridine pendants are situated alternatively above and below the main hole of the macrocycle. The related La(III) complex

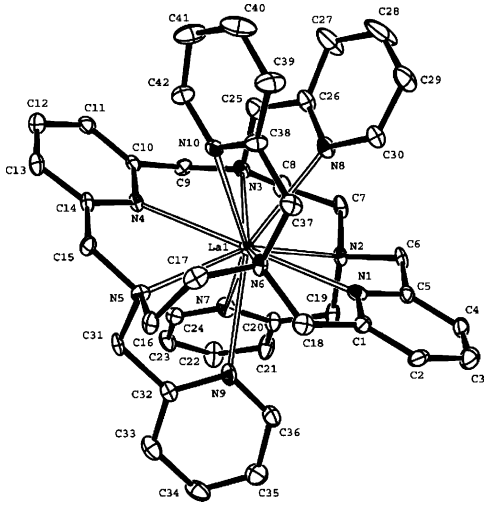

Figure 1. X-ray crystal structure of $[La(\mathbf{L})]^{3+}$ showing the atomic numbering scheme. Hydrogen atoms are omitted for simplicity. The ORTEP plot is at the 30% probability level.

with the ligand containing the same 18-membered hexaaza macrocyclic framework and four phosphonate pendant arms, $[La(H_5\mathbf{L^2})]$, as well as the La−Dy complexes of the tetraacetate pendant-armed ligand $\mathbf{L^1}$ (Chart 1), presents a similar 10-coordinate geometry.[28] The bond lengths of the metal coordination environment are comparable to the ranges previously observed for 10-coordinated lanthanide complexes.[29] The N−Ln bond distances in $[Ln(\mathbf{L})]^{3+}$ are slightly longer than the bond distances in the corresponding $[Ln(\mathbf{L^1})]^+$ complexes, while the La(III) complex shows similar N−La bond distances than those observed in $[La(H_5\mathbf{L^2})]$. The pyridine nitrogen atoms of the macrocyclic unit provide the strongest bond to the lanthanide ion in all the crystal structures obtained (Table 2). As usually seen, a progressive decrease of the Ln−donor-atom bond distances is observed upon decreasing the ionic radii of the lanthanide ions.[30] The exception comes from the $[Tm(\mathbf{L})]^{3+}$ complex, which shows longer distances of the metal coordination environment than the $[Er(\mathbf{L})]^{3+}$ one (Table 2). A similar enlargement of Ln−N bond distances along the lanthanide series has been previously observed for lanthanide complexes with azacrown ethers, which has been attributed to a better fit between the ligand cavity and the light Ln(III) ions.[31]

The dihedral angles between the pyridine rings of the macrocyclic framework varies between 12.8° for **12** and 17.8° for **11**, showing a slight twist of these pyridine units relative to each other, as also found for the lanthanide complexes with $\mathbf{L^1}$. The lanthanide ion is situated approximately in the best plane formed by the six nitrogen donor atoms of the macrocycle. This plane is however considerably distorted, with an average root mean square

(26) Gill, N. S.; Nuttall, R. H.; Scaife, D. E.; Sharp, D. W. *J. Nucl. Chem.* **1961**, *18*, 79.
(27) Carnall, W. T.; Siegel, S.; Ferraro, J. R.; Tani, B.; Gebert, E. *Inorg. Chem.* **1973**, *12*, 560.
(28) Bligh, S. W. A.; Choi, N.; Geraldes, C. F. G. C.; Knoke, S.; McPartlin, M.; Sanganee, M. J.; Woodroffe, T. M. *J. Chem. Soc., Dalton Trans.* **1997**, 4119.
(29) Alexander, V. *Chem. Rev.* **1995**, *95*, 273.
(30) Platas, C.; Avecilla, F.; de Blas, A.; Geraldes, C. F. G. C.; Rodríguez-Blas, T.; Adams, H.; Mahía, J. *Inorg. Chem.* **1999**, *38*, 3190.
(31) Platas, C.; Avecilla, F.; de Blas, A.; Rodríguez-Blas, T.; Bastida, R.; Macías, A.; Rodríguez, A.; Adams, H. *J. Chem. Soc., Dalton Trans.* **2001**, 1699.

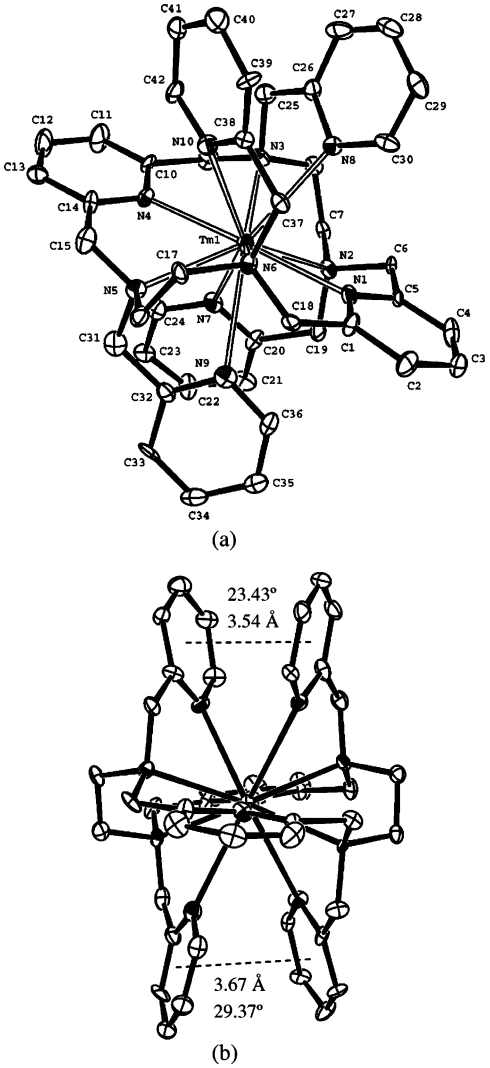

Figure 2. (a) X-ray crystal structure of $[Tm(\mathbf{L})]^{3+}$ showing the atomic numbering scheme; (b) view of the X-ray crystal structure of $[Tm(\mathbf{L})]^{3+}$ highlighting the intramolecular face-to-face π,π-interactions. Hydrogen atoms are omitted for simplicity. The ORTEP plot is at the 30% probability level.

(rms) deviation from planarity of 0.70 Å. As in the analogous 10-coordinate Ln(III) complexes of $\mathbf{L^1}$ and $\mathbf{L^2}$, the macrocyclic framework in all present structures shows virtually no folding, the angle between the pyridine nitrogen atoms of the ligand backbone and the lanthanide ion being around 175° in **1** and **2** and close to 179° in **3**, **7**, **8**, **11**, and **12**.

It is well-known that $[Ln(DOTA)(H_2O)]^-$ complexes exist as two enantiomeric pairs of diasteroisomers because they present two sources of helicity: one is due to the four five-membered rings formed by the binding of the acetate arms to the ion, and the other is due to the four five-membered rings formed by the binding of the macrocyclic cyclen unit.[32] Similarly, in the $[Ln(\mathbf{L})]^{3+}$ complexes each of the coordinated ethylenediamine units forms five-membered chelate rings that can adopt δ or λ conformations.[33] The conformation of these two five-membered chelate rings changes along the lanthanide series. In **1** and **2** the cation $[Ln(\mathbf{L})]^{3+}$ presents a $\lambda\delta$ (or $\delta\lambda$) conformation of these five-membered chelate rings, whereas in **3**, **7**, **8**, **11**, and **12** the cations show $\lambda\lambda$ (or $\delta\delta$) conformations. In all cases the amine nitrogen atoms show *SSSS* or *RRRR* configurations, since both enantiomers are present in the crystal.

This series of lanthanide complexes displays interesting structural features. Inspection of the crystal structures obtained reveals that face-to-face π,π-interactions are established between pairs of pyridine pendant groups (Figure 2b).[34] The La(III) and Ce(III) complexes, which display the same ($\lambda\delta$ or $\delta\lambda$) configuration, show similar values of the dihedral angles between the two pairs of π,π-stacked pyridine groups (ca. 48° and 23°). In the other $[Ln(\mathbf{L})]^{3+}$ complexes (Ln = Pr, Gd, Tb, Er, and Tm), these dihedral angles are smaller than in the La(III) and Ce(III) complexes, varying between 14° in Tb(III) and 29° in Tm(III). The distances between centroids of the pendant aromatic rings range from 3.2 to 4.0 Å. Similar π,π-stacking interactions have been previously observed in complexes of macrocyclic ligands containing two pendant arms.[35] The presence of these intramolecular interactions leads to the formation of a cryptlike cavity that enhances the stability of the complex.[36] This effect may be responsible for the stabilization of the 10-coordinate geometry in $[Ln(\mathbf{L})]^{3+}$ complexes. Indeed, while the Er(III) and Tm(III) complexes of $\mathbf{L^1}$ are 9-coordinate, with only three of the four pendant arms coordinated to the metal ion, the corresponding $[Ln(\mathbf{L})]^{3+}$ complexes are 10-coordinate. Thus, in the $[Ln(\mathbf{L})]^{3+}$ complexes 10-coordinate structures are still favorable for small lanthanide ions such as Er(III) and Tm(III), which can be attributed to the presence of π,π-stacking interactions between the two pairs of pyridine pendants.

The coordination polyhedron around the Ln(III) ion can be described in all cases as a bicapped square antiprism (Figure 3). For **1**−**3**, the square faces of the antiprism are composed of the two parallel planes formed by N(1), N(2), N(7), and N(9) and by N(3), N(5), N(6), and N(8), while N(10) is capping one of the square faces of the square antiprism and N(4) is capping one of the triangular faces. However, in **7**, **8**, **11**, and **12**, the previous planes present large rms deviations from planarity, and the antiprism may be considered to be comprised by the two parallel planes formed by N(2), N(6), N(8), and N(9) and by N(3), N(5), N(7), and N(10), with N(1) and N(4) capping both square faces of the antiprism. The rms values of the two parallel planes are near 0.1 Å in all cases.

The anion complexes $[Ln(NO_3)_m(H_2O)_n]^{x-}$ (Ln = La, Ce, Pr, Gd, Tb, Er, and Tm) show the metal ion bound to a

(32) (a) Aime, S.; Botta, M.; Ermondi, G. *Inorg. Chem.* **1992**, *31*, 4291. (b) Aime, S.; Botta, M.; Fasano, M.; Marques, M. P. M.; Geraldes, C. F. G. C.; Pubanz, D.; Merbacch, A. E. *Inorg. Chem.* **1997**, *36*, 2059.

(33) Rodríguez-Cortiñas, R.; Avecilla, F.; Platas-Iglesias, C.; Imbert, D.; Bünzli, J.-C. G.; de Blas, A.; Rodríguez-Blas, T. *Inorg. Chem.* **2002**, *41*, 5336.

(34) (*a*) Hunter C. A.; Sanders, J. K. M. *J. Am. Chem. Soc.* **1990**, *112*, 5525. (*b*) Song, R.-F.; Xie, Y.-B.; Li J.-R.; Bu, X.-H. *J. Chem. Soc., Dalton Trans.* **2003**, 4742.

(35) Gonzalez-Lorenzo, M.; Platas-Iglesias, C.; Avecilla, F.; Geraldes, C. F. G. C.; Imbert, D.; Bünzli, J.-C. G.; de Blas, A.; Rodríguez-Blas, T. *Inorg. Chem.* **2003**, *42*, 6946.

(36) Zhang, X.-X.; Boedunov, A. V.; Bradshaw, J. S.; Dalley, N. K.; Kou, X.; Izatt, R. M. *J. Am. Chem. Soc.* **1995**, *117*, 11507.

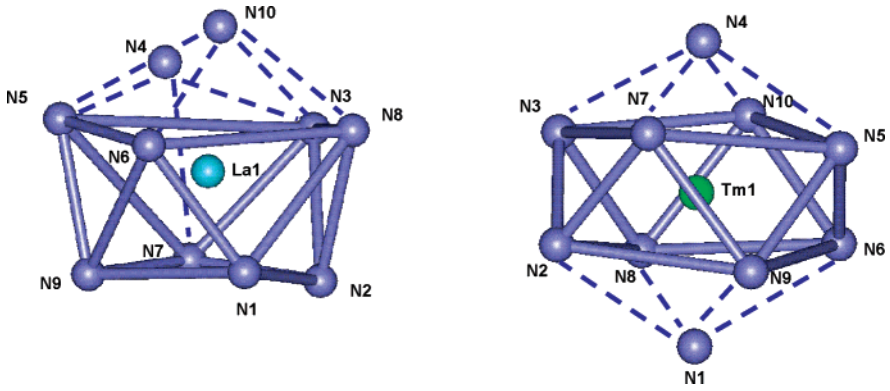

Figure 3. Coordination polyhedra of complexes $[La(\mathbf{L})]^{3+}$ (left) and $[Tm(\mathbf{L})]^{3+}$ (right).

different number of oxygen atoms of nitrate groups and water molecules. For Ln = La, Ce, Pr, and Tb, the metal ions are bound to 12 oxygen atoms of 6 bidentate nitrate groups in a distorted icosahedral geometry. For Ln = Gd, the coordination number is 10 and the metal ion is surrounded by four bidentate nitrate groups and two water molecules, giving rise to a distorted bicapped antiprism. Finally, for the smaller Er and Tm ions, the coordination number is 9 arising from three bidentate nitrate groups and three water molecules in a monocapped antiprism environment.

DFT Calculations. The $[Ln(\mathbf{L})]^{3+}$ systems (Ln = La, Pr, Eu, Tb, or Tm) were investigated by means of DFT calculations (B3LYP model). As there is not a good all-electron basis set for lanthanides, the effective core potential (ECP) of Dolg et al.[23] and the related [5s4p3d]-GTO valence basis set were applied in these calculations. This ECP includes $46 + 4f^n$ electrons in the core, leaving the outermost 11 electrons to be treated explicitly, and it has been demonstrated to provide reliable results for several lanthanide complexes with both macrocyclic[37,38] or acyclic[39−41] ligands. Compared to all-electron basis sets, ECPs account to some extent for relativistic effects, which are believed to become important for the elements from the fourth row of the periodic table. Two geometries of the complexes showing different conformations of the two five-membered chelate rings formed by the ethylenediamine moieties were considered: $\delta\lambda$ and $\lambda\lambda$. The calculated structures of the $\delta\lambda$ complexes show C_2 symmetry, the symmetry axis passing through the center of the C−C bonds of the ethylenediamine moieties, while the calculated structures of the $\lambda\lambda$ complexes display D_2 symmetry. Calculated bond distances of the metal coordination environment are compared with the experimental data obtained from X-ray analyses in Table 3. The calculated distances between the lanthanide and the donor atoms of the macrocyclic unit are in excellent agreement with the experimental values (within 0.01−0.06 Å), while the calculated distances to the donor atoms of the pendant arms are slightly longer than the experimental values (ca. 0.03−0.07 Å). Optimized Cartesian coordinates obtained for the different $[Ln(\mathbf{L})]^{3+}$ systems are given in the Supporting Information. Analogous calculations performed at the HF level (data not shown) provide distances between the lanthanide ion and the donor atoms of the pendant arms 0.03−0.04 Å longer than those obtained from B3LYP calculations. Thus, the introduction of electron correlation effects improves the agreement between calculated and experimental geometries of $[Ln(\mathbf{L})]^{3+}$ complexes. For a given lanthanide complex the $\lambda\lambda$ conformation shows shorter

Table 3. Values of the Mean Distances (Å) of Experimental and Calculated Structures of the Two Isomers of $[Ln(\mathbf{L})]^{3+}$ Complexes[a]

		$\delta\lambda$ isomer		$\lambda\lambda$ isomer	
		exptl	calcd	exptl	calcd
La	La−$N_{PY(m)}$	2.694(0.017)	2.749(0.000)		2.658(0.000)
	La−N_{AM}	2.766(0.034)	2.812(0.004)		2.752(0.000)
	La−$N_{PY(p)}$	2.790(0.045)	2.824(0.014)		2.897(0.000)
	$N_{PY(m)}$−$N_{PY(m)}$	5.382	5.492		5.317
Ce	Ce−$N_{PY(m)}$	2.688(0.019)			
	Ce−N_{AM}	2.753(0.019)			
	Ce−$N_{PY(p)}$	2.768(0.071)			
	$N_{PY(m)}$−$N_{PY(m)}$	5.369			
Pr	Pr−$N_{PY(m)}$		2.735(0.000)	2.614(0.003)	2.637(0.000)
	Pr−N_{AM}		2.795(0.005)	2.687(0.008)	2.732(0.000)
	Pr−$N_{PY(p)}$		2.795(0.017)	2.803(0.042)	2.876(0.000)
	$N_{PY(m)}$−$N_{PY(m)}$		5.463	5.226	5.275
Eu	Eu−$N_{PY(m)}$		2.713(0.000)		2.603(0.000)
	Eu−N_{AM}		2.770(0.006)		2.702(0.000)
	Eu−$N_{PY(p)}$		2.748(0.022)		2.842(0.000)
	$N_{PY(m)}$−$N_{PY(m)}$		5.420		5.206
Gd	Gd−$N_{PY(m)}$			2.542(0.010)	
	Gd−N_{AM}			2.657(0.015)	
	Gd−$N_{PY(p)}$			2.784(0.020)	
	$N_{PY(m)}$−$N_{PY(m)}$			5.083	
Tb	Tb−$N_{PY(m)}$		2.705(0.000)	2.548(0.002)	2.588(0.000)
	Tb−N_{AM}		2.762(0.007)	2.659(0.010)	2.690(0.000)
	Tb−$N_{PY(p)}$		2.725(0.024)	2.770(0.068)	2.829(0.000)
	$N_{PY(m)}$−$N_{PY(m)}$		5.403	5.096	5.177
Er	Er−$N_{PY(m)}$			2.530(0.006)	
	Er−N_{AM}			2.639(0.022)	
	Er−$N_{PY(p)}$			2.750(0.075)	
	$N_{PY(m)}$−$N_{PY(m)}$			5.058	
Tm	Tm−$N_{PY(m)}$		2.693(0.000)	2.555(0.018)	2.564(0.000)
	Tm−N_{AM}		2.745(0.007)	2.654(0.015)	2.669(0.000)
	Tm−$N_{PY(p)}$		2.693(0.031)	2.771(0.086)	2.811(0.000)
	$N_{PY(m)}$−$N_{PY(m)}$		5.378	5.108	5.128

[a] The average values are reported with standard deviations in parentheses. $N_{PY(m)}$, pyridine nitrogen atoms of the macrocyclic unit; N_{AM}, amine nitrogen atoms; $N_{PY(p)}$, pyridine nitrogen atoms of the pendant arms.

(37) Gonzalez-Lorenzo, M.; Platas-Iglesias, C.; Avecilla, F.; Faulkner, S.; Pope, S. J. A.; de Blas, A.; Rodriguez-Blas, T. *Inorg. Chem.* **2005**, *44*, 4254.
(38) Cosentino, U.; Villa, A.; Pitea, D.; Moro, G.; Barone, V.; Maiocchi, A. *J. Am. Chem. Soc.* **2002**, *124*, 4901.
(39) Platas-Iglesias, C.; Mato-Iglesias, M.; Djanashvili, K.; Muller, R. N.; Vander Elst, L.; Peters, J. A.; de Blas, A.; Rodríguez-Blas, T. *Chem.—Eur. J.* **2004**, *10*, 3579.
(40) Quali, N.; Bocquet, B.; Rigault, S.; Morgantini, P.-Y.; Weber, J.; Piguet, C. *Inorg. Chem.* **2002**, *41*, 1436.
(41) Mato-Iglesias, M.; Platas-Iglesias, C.; Djanashvili, K.; Peters, J. A.; Tóth, É.; Balogh, E.; Muller, R. N.; Vander Elst, L.; de Blas, A.; Rodríguez-Blas, T. *Chem. Commun.* **2005**, 4729.

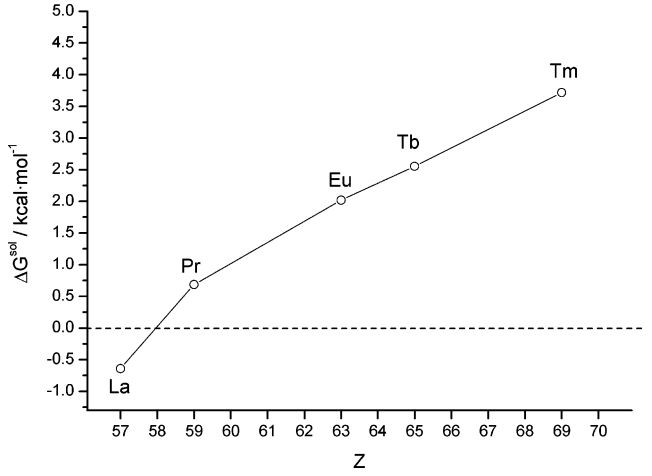

Figure 4. In aqueous solution C-PCM relative free energy of the $\delta\lambda$ isomer ($\Delta G^{sol} = G^{sol}_{(\delta\lambda)} - G^{sol}_{(\lambda\lambda)}$) in $[Ln(\mathbf{L})]^{3+}$ complexes.

distances between the lanthanide ion and the donor atoms of the macrocyclic unit than the $\delta\lambda$ one. On the contrary, the $\delta\lambda$ conformation shows stronger interactions of the lanthanide ion with the donor atoms of the pendant arms (Table 3).

The relative free energies of the $\delta\lambda$ and $\lambda\lambda$ conformations of $[Ln(\mathbf{L})]^{3+}$ complexes were calculated in aqueous solution by using the B3LYP model and the 6-311G** basis set for the ligand atoms. It has been demonstrated that this computational approach provides relative energies of the two isomers of $[Ln(DOTA)(H_2O)]^-$ in close agreement to the experimental ones.[38] Relative free energies were calculated as $\Delta G^{sol} = G^{sol}(\delta\lambda) - G^{sol}(\lambda\lambda)$, and therefore a positive relative energy indicates that the $\lambda\lambda$ conformation is more stable than the $\delta\lambda$ one. Our results (Figure 4) indicate that the relative energy of the $\delta\lambda$ conformation increases along the lanthanide series. The $\delta\lambda$ conformation is the most stable one in the case of the La(III) complex, while for Pr(III), Eu(III), Tb(III), and Tm(III) complexes the minimum energy conformation corresponds to the $\lambda\lambda$ form. Thus, our calculations predict a minimum energy conformation that corresponds to that found experimentally in the solid state. The stabilization of the $\lambda\lambda$ geometry on decreasing the ionic radius of the lanthanide ion can be explained because this conformation favors a smaller macrocyclic cavity of the ligand than the $\delta\lambda$ one. Indeed, the $\lambda\lambda$ geometries show shorter distances between both nitrogen atoms of the pyridine units of the macrocycle than the $\delta\lambda$ ones (Table 3).

Proton NMR Spectra. The ^{1}H NMR spectra of the $[Ln(\mathbf{L})]^{3+}$ complexes were obtained in D_2O solution at pD = 6 (Figure 5). The assignments of the proton signals of the diamagnetic La(III) and Y(III) complexes were aided with standard 2D homonuclear COSY experiments, which gave strong cross-peaks between the geminal $-CH_2-$ protons and between ortho-coupled pyridyl protons. The diamagnetic spectra consist of 12 multiplets corresponding to the 12 different proton magnetic environments of the ligand backbone, which points to an effective D_2 symmetry of the complexes in solution (Figure 5). Although the specific CH_2 proton assignments, H3ax/H3eq, H4ax/H4eq, and H5a/H5b, were not possible on the basis of the 2D NMR spectra, they

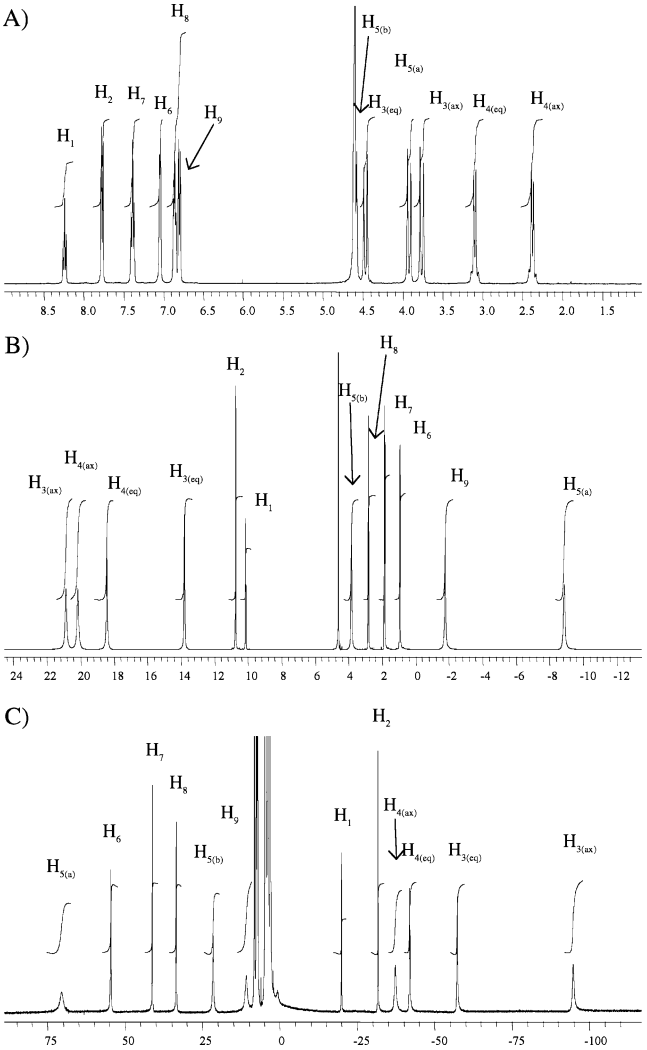

Figure 5. ^{1}H NMR (400 MHz) spectra of the $[Ln(\mathbf{L})]^{3+}$ complexes in D_2O solution (pD = 6.0): (A) La(III) complex; (B) Ce(III) complex; (C) Yb(III) complex.

were carried out using the stereochemically dependent proton shift effects, resulting from the polarization of the C−H bonds by the electric field effect caused by the cation charge.[42] This results in a deshielding effect of the H3eq, H4eq, and H5b protons, which are pointing away from the Ln(III) ion (Table 4, see Chart 1 for labeling). The methyleneprotons H3ax/H3eq and H5a/H5b yield AB spin patterns, while the protons of the ethylenediamine units H4ax/H4eq give an AA′BB′ spectrum. The spectra show the signals of the H6 and H9 protons of the pendant arms at relatively low frequencies. Inspection of the X-ray structure of compound **1** shows that these protons are directed toward the aromatic ring current of the neighbor pendant arm. Thus, the low-frequency shift observed for these protons is attributable to a ring current shift effect provoked by the pyridine ring, which results in a shielding for any nuclei above or below this ring. These results indicate that the complexes maintain in solution the *SSSS* (or *RRRR*) configuration observed in the solid-state structures, where face-to-face π,π-interactions

(42) Harris, R. K. *Nuclear Magnetic Resonance Spectroscopy: A Physicochemical View;* Pitman: London, 1983.

Table 4. ^{1}H NMR Shifts (ppm) Observed for $[Ln(\mathbf{L})]^{3+}$ Complexes in D_2O Solution at pD = 6[a]

	H1	H2	H3(ax)	H3(eq)	H4(ax)	H4(eq)	H5(a)	H5(b)	H6	H7	H8	H9
La[a]	8.29	7.82	3.80	4.53	2.43	3.16	3.90	4.67	7.09	7.44	6.91	6.84
Y[b]	8.28	7.78	3.59	4.40	2.29	2.98	3.85	4.55	6.68	7.37	6.89	6.68
Ce	10.20	10.83	21.36	14.09	20.70	18.92	−9.13	3.90	0.88	1.77	2.76	−1.98
Pr	17.33	20.62	35.70	26.23	19.53	26.52	−16.87	2.42	−7.55	−3.25	−2.27	1.78
Nd	18.50	21.18	21.72	20.86	14.26	14.64	−5.94	1.93	2.49	0.13	−3.55	−0.44
Sm	9.14	9.14	6.28	9.73	4.03	6.05	1.17	2.81	4.03	5.68	5.31	5.25
Tb	48.9	76.3	286.0	141.5	212.0	134.8	−188.5	−30.73	−111.5	−75.4	−79.1	−95.5
Tm	−39.9	−66.6	−239.8	−140.7	−151.0	−148.2	175.6	22.7	111.9	83.7	72.1	51.1
Yb	−19.5	−31.6	−94.7	−57.3	−37.3	−41.8	70.6	21.6	54.6	41.2	33.5	10.8

[a] $^3J_{1-2}$ = 8.1 Hz; $^3J_{9-8}$ = 7.7 Hz; $^3J_{6-7}$ = 5.3 Hz; $^2J_{3ax-3eq}$ = 17.5 Hz; $^2J_{4ax-4eq}$ = 10.6 Hz; $^2J_{5a-5b}$ = 16.3 Hz. [b] $^3J_{1-2}$ = 7.9 Hz; $^2J_{3ax-3eq}$ = 17.4 Hz; $^2J_{4ax-4eq}$ = 10.2 Hz; $^2J_{5a-5b}$ = 16.7 Hz.

are established between pairs of pyridine pendant groups. The ^{1}H NMR spectrum of the binuclear Cd(II) complex of **L**, for which no π,π-interactions have been observed in the solid state, shows the signals due to the H6 and H9 protons at 8.17 and 7.58 ppm, respectively.[43]

The ^{1}H NMR spectra of the paramagnetic Ce(III), Pr(III), Nd(III), and Sm(III) complexes show relatively sharp signals that could be partially assigned with the aid of standard 2D homonuclear COSY experiments. A full assignment of the spectra was achieved by using the shift-analysis method developed by Forsberg.[18] The shift-analysis program permutes the lanthanide induced shift values (LIS) over any number of selected nuclei, determining which particular assignment of peaks gives the best fit to the LIS data (see later). The ^{1}H NMR spectra of the Tb(III), Tm(III), and Yb(III) complexes could be also fully assigned by using the shift-analysis method and line-width analyses (Table 4). The ^{1}H NMR spectra of the paramagnetic complexes consist of 12 signals corresponding to the 12 different proton magnetic environments of the ligand backbone, which points again to an effective D_2 symmetry of the complexes in solution (Figure 5).

Lanthanide Induced Shifts (LIS). The binding of a ligand to a paramagnetic Ln(III) ion generally results in large NMR frequency shifts at the ligand nuclei, with magnitudes and signs depending critically on both the nature of the lanthanide ion and the location of the nucleus relative to the metal center.[11] Thus, the analysis of the NMR spectra of Ln(III) paramagnetic complexes can provide useful structural information in solution. For a given nucleus *i*, the isotropic paramagnetic shift induced by a lanthanide ion *j* (δ_{ij}^{para}) is generally a combination of the Fermi contact (δ_{ij}^{con}) and dipolar (δ_{ij}^{dip}) contributions:[11]

$$\delta_{ij}^{para} = \delta_{ij}^{exp} - \delta_{i}^{dia} = \delta_{ij}^{con} + \delta_{ij}^{dip} \qquad (2)$$

where the diamagnetic contribution δ_i^{dia} is obtained by measuring the chemical shifts for analogous diamagnetic complexes (the La(III) complex in the present case). Generally, the contact contribution quickly diminishes as the number of bonds between a given Ln(III) and the monitored nucleus increases. We therefore initiated the analysis of the paramagnetic shifts with the assumption that they are dominated by dipolar contributions, as given by the following equation:

$$\delta_{ij}^{dip} = D_1 \frac{3\cos^2\theta - 1}{r^3} + D_2 \frac{\sin^2\theta \cos 2\varphi}{r^3} \qquad (3)$$

where r, θ, and φ are the spherical coordinates of the observed nucleus with respect to Ln(III) at the origin and D_1 and D_2 are proportional, respectively, to the axial [$\chi_{zz} - {}^1/_3(\chi_{xx} + \chi_{yy} + \chi_{zz})$] and rhombic ($\chi_{xx} - \chi_{yy}$) anisotropies of the magnetic susceptibility tensor $\boldsymbol{\chi}$. In the special case of axial symmetry the second term of eq 3 vanishes since $D_2 = 0$.

The analysis of the paramagnetic shifts to get structural information is generally initiated by assuming some structure for the complex in solution, thereby allowing the calculation of the geometric factors. A common practice is to assume that the structure in solution is the same as that determined in the solid state by X-ray crystallography,[30] and an alternative approach is to use molecular[44,45] or quantum[39] mechanical calculations to approximate the structure of a complex. The Cartesian coordinates of the Tm(III) complex, as well as the calculated DFT geometries in both $\delta\lambda$ and $\lambda\lambda$ conformations, were used to assess the agreement between the experimental and predicted Ln(III)-induced paramagnetic shifts for the $[Ln(\mathbf{L})]^{3+}$ complexes of the second part of the lanthanide series (Ln = Tb−Yb). For the light lanthanide complexes (Ln = Ce−Eu), the X-ray crystal structures of the Ce(III) and Pr(III) complexes, which show respectively $\delta\lambda$ and $\lambda\lambda$ conformations, as well as the calculated geometries of the Pr(III) complex, were used as input geometries. Good fits according to the dipolar model are expected for those Ln(III) complexes where the lowest theoretical contact contributions are expected. Thus, we performed an analysis of the paramagnetic shifts observed for the Ce(III), Tm(III), and Yb(III) complexes, for which the theoretical ratio of the contact and dipolar contributions is lower than 0.155.[11] The shift-analysis program calculates the dipolar shifts defined by eq 3 in the molecular coordinate system by using a linear least-squares search that minimizes the difference between the experimental and calculated data. The agreement between the experimental and calculated data by using X-ray crystal

(43) Fernández-Fernández, M. C.; Bastida, R.; Macías, A.; Valencia, L.; Pérez-Lourido, P. *Polyhedron* **2006**, *25*, 783.

(44) Di Bari, L.; Pescitelli, G.; Sherry, A. D.; Woods, M. *Inorg. Chem.* **2005**, *44*, 8391.

(45) Platas-Iglesias, C.; Piguet, C.; Andre, N.; Bünzli, J.-C. G. *J. Chem. Soc., Dalton Trans.* **2001**, 3084.

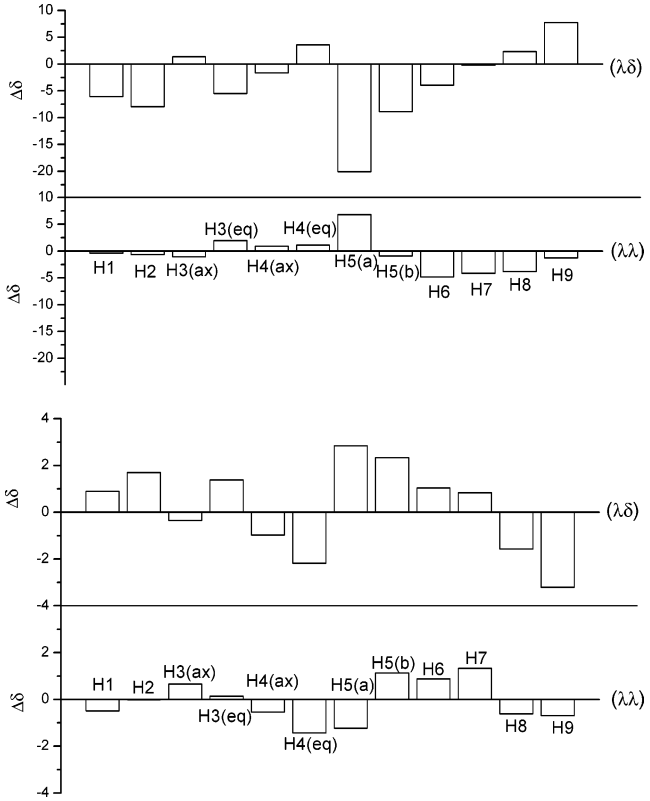

Figure 6. Plot of the differences between experimental and calculated shift values ($\Delta\delta$) for the right [($\lambda\lambda$)] and wrong [($\delta\lambda$)] solution structures of the [Yb(**L**)]$^{3+}$ (top) and [Ce(**L**)]$^{3+}$ (bottom) complexes.

structures or B3LYP calculated structures is very similar, the calculated AF_j factors differing by less than 0.004 units. We therefore performed the analysis of the LIS values by using the calculated structures, since they show nearly undistorted geometries (Table 3), which allows us to easily locate the principal magnetic axis system of the complexes (see later). On the contrary, X-ray structures are more distorted because of crystal packing forces in the solid state (Table 3), which result in slightly different values of the geometrical factors (eq 3) for magnetically equivalent protons and thus result in different calculated dipolar shifts that must be averaged for comparison with the experimental values.

The agreement between the experimental and calculated isotropic shifts of the Tm(III) and Yb(III) complexes obtained by using the [Tm(**L**)]$^{3+}$ calculated structure showing $\delta\lambda$ conformation is rather poor [$AF_j > 0.19$, eq 1]. However, much better agreement factors are obtained for the complexes in $\lambda\lambda$ conformation [$AF_j < 0.07$, eq 1]. Figure 6 shows a plot of differences between experimental and calculated shift values ($\Delta\delta$) for the [Yb(**L**)]$^{3+}$ complex, where it is possible to appreciate large deviations from the experimental values for the H1, H2, H5(a), and H9 protons of the $\delta\lambda$ form. These results indicate that these complexes present a $\lambda\lambda$ conformation in aqueous solution, in agreement with the solid-state structure of **12**. A similar situation occurs for the Ce(III) complex, a plot of the differences between experimental and calculated shift values ($\Delta\delta$) showing a better agreement for the $\lambda\lambda$ conformation ($AF_j = 0.083$) than for the $\delta\lambda$ one ($AF_j = 0.204$). Moreover, a plot of $\Delta\delta$ for the [Ce(**L**)]$^{3+}$ complex shows large deviations from the experimental values for the H2, H5(a), and H9 protons of the $\delta\lambda$ form. This indicates that Ce(III) complexes present a $\lambda\lambda$ conformation in aqueous solution, while the X-ray crystal structure of **2** shows a $\delta\lambda$ conformation of the complex in the solid state. Thus, the [Ln(**L**)]$^{3+}$ complexes present a $\lambda\lambda$ conformation along the whole lanthanide series from Ce(III) to Yb(III).

The agreement factors obtained for the Ce(III), Tm(III), and Yb(III) complexes in $\lambda\lambda$ conformation are excellent ($AF_j < 0.085$, Table 5), indicating good fits of the experimental data according to the dipolar model. Similar agreement factors were previously obtained for different Yb(III) and/or Tm(III) complexes according to the dipolar model.[46] Interestingly, poorer agreement factors between experimental and calculated shifts are often observed even when a separation of the contact contributions to the observed LIS has been performed. For instance, for the [Ce(**L**^{1})]$^{3+}$ complex an agreement factor $AF_j = 0.113$ has been obtained,[10] with contact contributions being factored out by using the Reilley method.[47] These results indicate (i) that the observed LIS values for the Ce(III), Tm(III), and Yb(III) complexes are largely dipolar in origin and (ii) that the B3LYP optimized geometries are good models for the structure in solution of the complexes. Less acceptable fits according to the dipolar model are obtained in those [Ln(**L**)]$^{3+}$ complexes where relatively important shift effects are predicted. For instance, we have obtained AF_j values of ca. 0.13 for the Pr(III) and Tb(III) complexes (Table 5), for which the theoretical ratios of the contact and dipolar contributions are 0.27 (Pr) and -0.37 (Tb).[11] Thus, contact shifts, although not dominant, appear to be relatively important for these complexes. Finally, an unacceptable fit according to the dipolar model ($AF_j = 0.322$) has been obtained for the Nd(III) complex, for which the theoretical ratio of the contact and dipolar contribution is 1.06. This indicates important contact contributions to the LIS values for the [Nd(**L**)]$^{3+}$ system.

Table 5 shows the D_1 and D_2 values providing the best fit of the experimental LIS values according to the dipolar model. The starting molecular axis system had the Ln(III) ion at the origin, with the *y* axis containing the pyridine nitrogen atoms of the macrocycle, the *x* axis being perpendicular to the best plane defined by the six macrocycle nitrogen atoms, and the *z* axis passing through the center of the C−C bonds of the ethylenediamine units (Figure 7). Thus, the molecular axis system chosen is coincident with the three C_2 axis of the molecule within the D_2 point group. In principle, another choice of axis would provide the same agreement factors between the experimental and calculated data. The values of D_1 and D_2, however, would end up being different.

As expected for a nonaxial system, the χ susceptibility tensor obtained in the molecule fixed axis system was rhombic, and was diagonalized in each case, providing a set of Euler angles that relate the principal magnetic axis system

(46) Lisowski, J.; Sessler, J. L.; Lynch, V.; Mody, T. D. *J. Am. Chem. Soc.* **1995**, *117*, 2273.
(47) Reilley, C. N.; Good, B. W.; Desreux, J. F. *Anal. Chem.* **1975**, *47*, 2110.

Table 5. Comparison of Experimental and Calculated[a] Dipolar ^{1}H Shifts (ppm) in $[Ln(\mathbf{L})]^{3+}$ Complexes[b]

	$[Ce(\mathbf{L})]^{3+}$		$[Pr(\mathbf{L})]^{3+}$		$[Tb(\mathbf{L})]^{3+}$		$[Tm(\mathbf{L})]^{3+}$		$[Yb(\mathbf{L})]^{3+}$	
	exptl	calcd	exptl	calcd	exptl	calcd	exptl	calcd	exptl	calcd
H1	−1.91	−1.42	−9.04	−8.12	−40.6	−44.9	48.2	49.3	27.8	28.2
H2	−3.01	−3.00	−12.80	−11.89	−68.5	−72.1	74.4	75.5	39.4	40.1
H3(ax)	−17.56	−18.22	−31.90	−34.17	−282.2	−270.3	243.6	245.9	98.5	99.6
H3(eq)	−9.56	−9.70	−21.70	−20.12	−137.0	−152.0	145.2	141.0	61.8	60.0
H4(ax)	−18.27	−17.73	−17.10	−17.51	−209.6	−193.1	153.4	151.9	39.7	38.8
H4(eq)	−15.75	−14.33	−23.36	−17.74	−131.6	−170.8	151.4	140.8	45.0	43.8
H5(a)	13.03	14.26	20.77	23.95	192.4	208.5	−171.7	−189.6	−66.7	−73.5
H5(b)	0.77	−0.36	2.25	3.44	35.4	16.49	−18.0	−23.4	−16.9	−16.0
H6	6.21	5.33	14.64	13.12	118.6	95.8	−104.8	−93.3	−47.5	−42.7
H7	5.67	4.34	10.69	9.68	82.8	71.3	−76.3	−67.2	−33.8	−29.6
H8	4.15	4.76	9.18	8.52	86.0	66.4	−65.2	−58.3	−26.6	−22.8
H9	8.82	9.51	5.06	7.31	102.3	81.5	−44.3	−49.0	−4.0	−2.69
D_1		−770		−939		−9025		7382		2280
D_2		1162		3178		21 198		−20 634		−9847
AF_j		0.083		0.133		0.133		0.064		0.063

[a] Calculated values were obtained by using the B3LYP/3-21G* optimized structures of the Pr(III), Tb(III), and Tm(III) complexes. [b] Positive values correspond to shifts to higher fields.

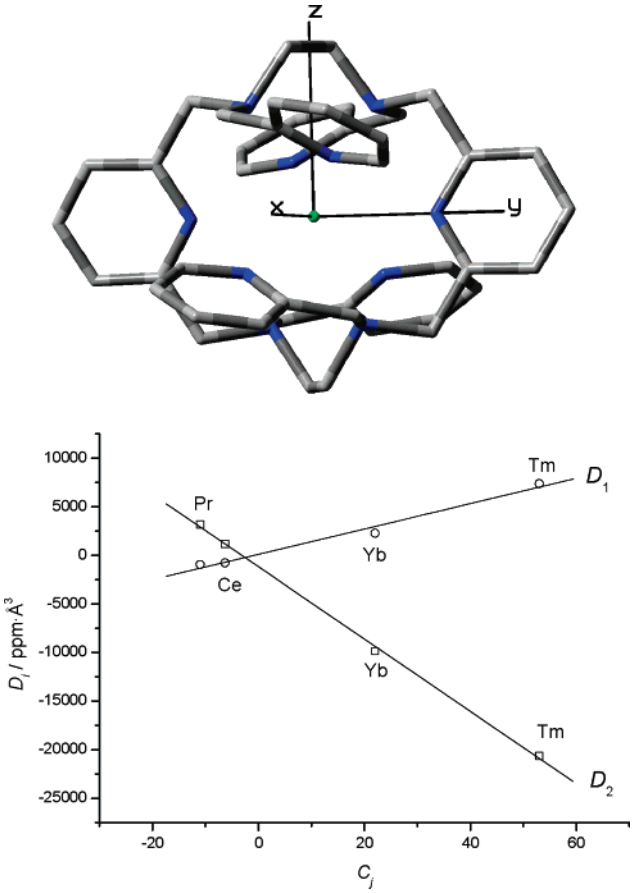

Figure 7. Top: display of the orientation of the magnetic susceptibility tensor of the $[Ln(\mathbf{L})]^{3+}$ complexes studied in this work. Bottom: correlation between the D_1 ($r^2 > 0.991$) and D_2 ($r^2 > 0.999$) values obtained for $[Ln(\mathbf{L})]^{3+}$ complexes and the theoretical C_J values.

to the molecular coordinate system. Our results show that the three Euler angles take values of zero, indicating that the magnetic axes are coincident with the molecular axes system chosen. The D_1 and D_2 constants (eq 3) are proportional to the following products:

$$D_1 \propto C_J A_2^0\langle r^2\rangle \quad \text{and} \quad D_2 \propto C_J A_2^2\langle r^2\rangle \tag{4}$$

where the $A_2^0\langle r^2\rangle$ and $A_2^2\langle r^2\rangle$ terms are the crystal field parameters, and C_J are numerical coefficients whose values are known for all lanthanides.[48] Plots of the D_1 and D_2 parameters versus the theoretical C_J values should be linear for a series of isostructural lanthanide complexes, providing that they possess comparable crystal field parameters.[49] This is indeed the case for the $[Ln(\mathbf{L})]^{3+}$ systems (Ln = Ce, Pr, Tm, and Yb), which demonstrate that these complexes present similar crystal field parameters (Figure 7). These results further confirm that these complexes present very similar solution structures and demonstrate the validity of the dipolar approximation for the analysis of the observed LIS values. For the Tb(III) complex, D_1 follows the linear correlation rather well, while D_2 is smaller than expected taking into account the theoretical C_J values, which suggests relatively important contact contributions for $[Tb(\mathbf{L})]^{3+}$.

Lanthanide Induced Relaxation Rates (LIR). The electron relaxation of the Ln(III) ions (excluding Gd(III)) is very fast ($T_{1e} \approx 10^{-13}$ s), and consequently, the contact contribution to the longitudinal ($1/T_1$) and transverse ($1/T_2$) paramagnetic relaxation is negligible. Two contributions are of importance: the "classical" dipolar relaxation and the Curie relaxation. Equations 5−7 can be derived from a simplified Solomon−Bloembergen equation[50] and the equation for the Curie relaxation (assuming extreme narrowing):[51,52]

$$\frac{1}{T_1} = \left[\frac{4}{3}a + \frac{6}{5}b\right]\frac{1}{r^6} \tag{5}$$

$$\pi\Delta\nu_{1/2} = \frac{1}{T_2} = \left[\frac{4}{3}a + \frac{7}{5}b\right]\frac{1}{r^6} \tag{6}$$

with

$$a = \left(\frac{\mu_0}{4\pi}\right)^2 \mu^2\gamma_I^2\beta^2 T_{1e} \quad \text{and} \quad b = \left(\frac{\mu_0}{4\pi}\right)^2 \frac{\gamma_I^2 H_0^2 \mu^4 \beta^4}{(3kT)^2}\tau_R \tag{7}$$

(48) Bleaney, B. *J. Magn. Reson.* **1972**, *8*, 91.
(49) Bertini, I.; Janik, M. B. L.; Lee, Y.-M.; Luchinat, C.; Rosato, A. *J. Am. Chem. Soc.* **2001**, *123*, 4181.
(50) Reuben, J.; Fiat, D. *J. Chem. Phys.* **1969**, *51*, 4918.

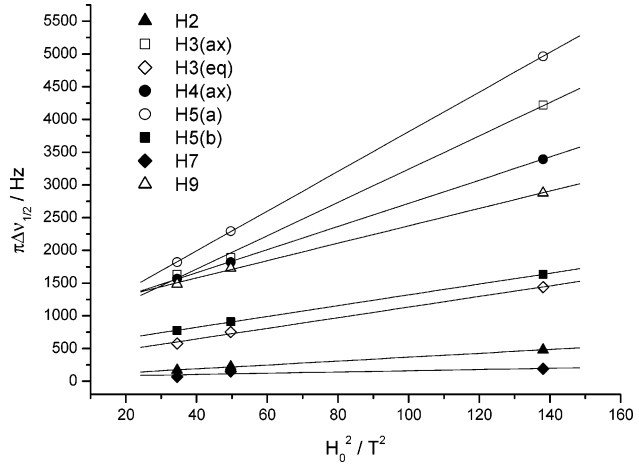

Figure 8. Plot of the line width of the $[Tb(\mathbf{L})]^{3+}$ resonances versus the square of the magnetic field strength. For clarity only data for selected nuclei is shown. The data were measured at 250, 300, and 500 MHz.

Here, $\mu_0/4\pi$ is the magnetic permeability in a vacuum, μ is the effective magnetic moment of the lanthanide ion, γ_I is the gyromagnetic ratio of the nucleus under study, β is the Bohr magneton, T_{1e} is the electron spin relaxation time, r is the distance between the ^{1}H nucleus in question and the lanthanide ion, H_0 is the magnetic field strength, k is the Boltzmann constant, T is the temperature, τ_R is the rotational tumbling time of the complex, and $\Delta\nu_{1/2}$ is the line width at half-height of a given resonance. The first term within brackets in eq 5 and eq 6 describes the contribution of the electron−nucleus dipolar interaction, while the second term describes the Curie-spin relaxation mechanism. According to the Curie contribution to $1/T_2$ (eq 6), the observed line widths should show a linear dependence upon the square of the applied magnetic field strength, with slopes that are proportional to the ratios of the inverse sixth power of the relevant metal−proton distances.[53] The observed line widths for the $[Tb(\mathbf{L})]^{3+}$ complex, as measured at 250, 300, and 500 MHz, show indeed a linear correlation with H_0^2 (Figure 8). Table 6 shows a comparison of the Tb···H distances obtained from the slope of these linear plots with those obtained for $[Tb(\mathbf{L})]^{3+}$ both experimentally (X-ray) and theoretically (DFT calculations). The experimental distances obtained from the LIR data have been determined by using H2 as an internal reference. The experimental distances obtained from the LIR data and those observed in the X-ray structure are in reasonably good agreement, while the agreement with the theoretical (DFT) distances is even better (within 0.3 Å for all protons except H9). This confirms that the calculated structure of $[Tb(\mathbf{L})]^{3+}$ is a good model of the solution structure of the complex. By using the experimental Tb···H distances shown in Table 6 and eq 6 and eq 7, we obtain $\tau_R = 203$ ps, a value that compares well with those obtained from nuclear magnetic relaxation dispersion (NMRD) studies for Gd(III) complexes of similar size and the same charge.[54] From the slopes of the plots shown in Figure 8 we obtain $T_{1e} = 4.1 \times 10^{-13}$ s, a value that is of the same order of magnitude as those determined for the aquaion[55] and other Tb(III) complexes.[53]

Table 6. Comparison of Relative Ln···H Distances (Å) Obtained from Experimental LIR Values with Those Obtained from DFT Calculations

	Ce	*Pr*	Tb		
	r_{exptl}[a]	r_{B3LYP}[b]	r_{exptl}[c]	r_{RX}[d]	r_{B3LYP}[e]
H1	6.72	6.51	6.30	6.37	6.47
H2	5.73	5.67	5.56	5.56	5.63
H3(ax)	3.47	3.71	3.88	3.59	3.69
H3(eq)	4.31	4.55	4.70	4.39	4.51
H4(ax)	3.56	3.86	4.13	3.71	3.84
H4(eq)	4.33	4.59	4.78	4.45	4.57
H5(a)	3.42	3.57	3.77	3.48	3.54
H5(b)	4.23	4.55	4.69	4.41	4.51
H6	5.72	5.75	5.93	5.56	5.71
H7	6.79	6.74	6.74	6.50	6.69
H8	6.18	6.00	6.18	5.81	5.96
H9	3.71	3.86	4.33	3.82	3.83

[a] Experimental values obtained from the measured T_1 values. [b] Values obtained from DFT calculations on the $[Pr(\mathbf{L})]^{3+}$ system in $\lambda\lambda$ conformation. [c] Experimental values obtained from the measured magnetic-field dependence of the line widths. [d] Calculated values from the crystal coordinates of $[Tb(\mathbf{L})]^{3+}$. [e] Values obtained from DFT calculations on the $[Tb(\mathbf{L})]^{3+}$ system.

At constant temperature and B_0, application of eq 5 and eq 7 allows the determination of absolute r values in the complexes providing that T_{1e} and τ_R are known. The proton $1/T_1$ values were determined for the $[Ce(\mathbf{L})]^{3+}$ complex (500 MHz) and corrected for the diamagnetic contribution by subtracting the relaxation rates of the same protons in the La(III) complex. The absolute Ce···H distances were obtained from the relaxation data by assuming the same τ_R value obtained for the Tb(III) complex (203 ps) and $T_{1e} = 1.8 \times 10^{-13}$ s (Table 6). The latter value corresponds to twice the value determined for the corresponding aquaion, as determined from the observed line widths for the Tb(III) analogue. It should be noted that because of the $1/r^6$ relationship, the accuracy of the estimated T_{1e} does not need to be very high to obtain accurate r values, an error of 30% in $1/T_{1e}$ corresponding to an error of only 5% in r. The analysis of the LIS data has revealed that the Ce(III) complex adopts a different structure in solution and in the solid state (see above) because of a different conformation of the five-membered chelate rings formed by the coordination of the ethylenediamine moieties. Thus, the experimental Ce···H distances obtained from the LIR data are compared in Table 6 with the B3LYP optimized distances calculated for the Pr(III) complex. The results show a good agreement between the experimental and calculated distances for these two systems. These results confirm that the DFT calculations presented in this paper provide an adequate description of the structure of the complexes in solution.

Conclusions

The structure of the lanthanide complexes of the tetrapyridyl pendant-armed macrocyclic ligand (**L**) has been studied

(51) Gueron, M. *J. Magn. Reson.* **1975**, *19*, 58.
(52) Vega, A. J.; Fiat, D. *Mol. Phys.* **1976**, *31*, 347.
(53) Aime, S.; Barbero, L.; Botta, M.; Ermondi, G. *J. Chem. Soc., Dalton Trans.* **1992**, 225.
(54) Caravan, P.; Ellinson, J. J.; McMurry, T. J.; Lauffer, R. B. *Chem. Rev.* **1999**, *99*, 2293.
(55) Alsaadi, B. M.; Rossotti, F. J. C.; Williams, R. J. P. *J. Chem. Soc., Dalton Trans.* **1980**, 2147.

in detail both in the solid state and in solution. The X-ray crystal structures of the La, Ce, Pr, Gd, Tb, Er, and Tm complexes show the metal ions being 10-coordinate, with the pyridine pendants situated alternatively above and below the main plane of the macrocycle. The conformations of the two five-membered chelate rings present in the complexes change along the lanthanide series. The La(III) and Ce(III) complexes show a $\lambda\delta$ (or $\delta\lambda$) conformation, while the complexes of the heavier lanthanide ions present $\lambda\lambda$ (or $\delta\delta$) conformation. The cationic $[Ln(\mathbf{L})]^{3+}$ complexes (Ln = La, Pr, Eu, Tb, and Tm) were also characterized by theoretical calculations at the DFT (B3LYP) level, by using the 3-21G* basis set for the ligand atoms and a $46 + 4f^n$ effective core potential for lanthanides. The structures obtained from these theoretical calculations are in very good agreement with the experimental solid-state structures. The theoretical calculations predict a stabilization of the $\lambda\lambda$ (or $\delta\delta$) conformation on decreasing the ionic radius of the Ln(III) ion, in agreement with the experimental evidence. The analysis of the LIS and LIR data demonstrates that the complexes maintain a 10-coordinate geometry in D_2O solution. The analysis of the LIS data unambiguously demonstrates that the Ce(III) complex presents a $\lambda\lambda$ (or $\delta\delta$) conformation in solution, while the solid-state structure shows a $\lambda\delta$ (or $\delta\lambda$) conformation. The LIS values are mainly dipolar in origin for the Ce(III), Tm(III), and Yb(III) complexes, and they are consistent with highly rhombic magnetic susceptibility tensors with the magnetic axes being coincident with the symmetry axes of the complexes.

Acknowledgment. We thank the Xunta de Galicia (Grant PGIDT04PXIB20901PR) for financial support. The authors are indebted to Centro de Supercomputación of Galicia (CESGA) for providing the computer facilities.

Supporting Information Available: X-ray crystallographic files, in CIF format; Table 1S, showing the dimensions (distances in Å, angles in deg) of the metal coordination spheres in compounds **1**−**3**, **7**, **8**, **11**, and **12**; Figures 1S−5S, showing ORTEP views of the X-ray crystal structures of **2**, **3**, **7**, **8**, and **11**; B3LYP optimized Cartesian coordinates (Å) of the $[Ln(\mathbf{L})]^{3+}$ systems (Ln = La, Pr, Eu, Tb, or Tm). This material is available free of charge via the Internet at http://pubs.acs.org.

IC0603508